

Hi Sebastian,

As we discussed many months ago we are approaching the comparison of Wally Van Orden's calculation with the measured  $A_{LT'}$  results differently than we have before. Below we outline the general idea and then go into the details.

The plan:

1. We want to compare the theoretical calculation of the helicity asymmetry  $A_{LT'}$  from Wally Van Orden with the asymmetry extracted from the data. The measured  $A_{LT'}$  is a function of the missing momentum  $p_m$ . We refer to Wally's calculation as WVO or  $A_{LT'}^{WVO}$ . He calculates the helicity asymmetry as a function of the missing momentum  $p_m$  at an array of values of  $Q^2$  and  $x_{Bj}$ . In other words  $A_{LT'}^{WVO} = A_{LT'}^{WVO}(p_m, Q^2, x_{Bj})$ . The measured helicity asymmetry we extract from the data is a function of  $p_m$  and integrated over the CLAS6 experimental acceptance in  $Q^2$  and  $x_{Bj}$ .
2. To properly compare the WVO calculation with the measured  $A_{LT'}$  we have to integrate the WVO calculation over the same distribution of  $Q^2$  and  $x_{Bj}$  as the data. We start by extracting the number of events as a function of  $Q^2$  and  $x_{Bj}$  which we call  $N(Q^2, x_{Bj})$  subject to the same cuts used to extract the measured  $A_{LT'}$ .
3. Next, we integrate  $N(Q^2, x_{Bj})$  over all  $Q^2$  and  $x_{Bj}$  and use the result as a normalization constant  $A$  to create a proper probability density  $P(Q^2, x_{Bj})$ .

$$A = \int_0^1 \int_0^\infty N(Q^2, x_{Bj}) dQ^2 dx_{Bj} \quad (1)$$

so

$$P(Q^2, x_{Bj}) = \frac{1}{A} N(Q^2, x_{Bj}) \quad (2)$$

4. We take each WVO calculation  $A_{LT'}^{WVO}(p_m, Q^2, x_{Bj})$  at a particular value of  $p_m$  (there are forty values of  $p_m$  in the WVO calculation) and construct its  $Q^2 - x_{Bj}$  surface. We then multiply each point on this surface by the appropriate probability density  $P(Q^2, x_{Bj})$ .
5. We then integrate over the  $Q^2$  and  $x_{Bj}$  ranges, *i.e.* add up the values for each  $Q^2$  and  $x_{Bj}$  at fixed  $p_m$ .

$$A_{LT'}^{WVO}(p_m) = \int_0^1 \int_0^\infty A_{LT'}^{WVO}(p_m, Q^2, x_{Bj}) \times P(Q^2, x_{Bj}) dQ^2 dx_{Bj} \quad (3)$$

This last result can now be compared with the measured  $A_{LT'}$ . In the steps we below we apply the procedure described in items 1-5.

Applying it:

- Consider the distribution of events  $N(Q^2, x_{Bj})$  that goes into the extraction of the measured  $A_{LT'}$  from the data as a function of  $Q^2$  and  $x_{Bj}$ . Those distributions  $N(Q^2, x_{Bj})$  are shown below in Fig 1 for the for 2.6 GeV, normal (left-hand panel) and reversed (right-hand panel) torus polarity settings. They were subject to the same cuts used to extract the measured  $A_{LT'}$  from the data.

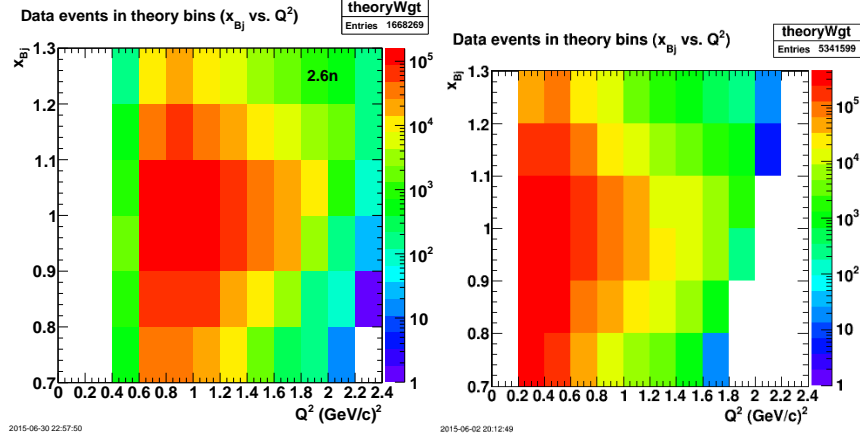


Figure 1: Raw  $N(Q^2, x_{Bj})$  for 2.6 GeV, normal polarity with the same cuts used for the measured  $A_{LT'}$  (left-hand panel) and for 2.6 GeV, reversed torus polarity (right-hand panel).

- Take the 2D distributions above (from ROOT) and read them into *Mathematica*. *Mathematica* has some nice interpolating functions so we can match the binning of the WVO calculation and the data (Wally varies his bin sizes at times). The panels in Fig 2 below show the results for the raw, discrete points (left-hand panel) and the interpolated surface in *Mathematica* (right-hand panel). Both panels in the figure were subject to the

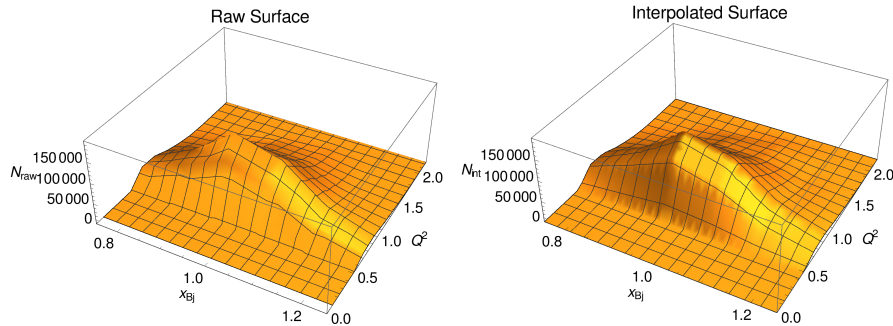


Figure 2: Surface plots of  $N(Q^2, x_{Bj})$  for 2.6 GeV, normal torus polarity for raw data (left-hand panel) and interpolated surface (right-hand panel).

same cuts as the data. The similarity of the two panels is a check on the interpolation.

8. The next figure, Fig 3, shows the same distributions discussed in part 7, but for the 2.6 GeV, reversed torus polarity data (compare with Fig 2). The interpolation is again consistent with the raw data.

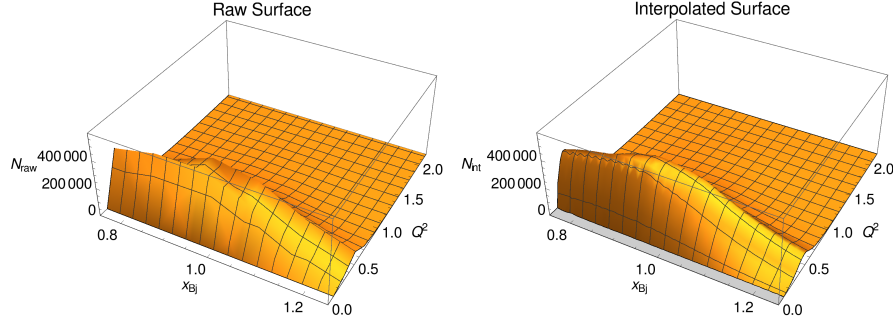


Figure 3: Surface plots of  $N(Q^2, x_{Bj})$  for the 2.6 GeV, reversed-polarity raw data (left-hand panel) and the interpolated surface (right-hand panel).

9. Now consider the WVO calculation  $A_{LT'}^{WVO}(p_m, Q^2, x_{Bj})$ . For each value of  $p_m$  in the calculation we construct a surface in  $Q^2$  and  $x_{Bj}$ . There are forty values of  $p_m$  in the WVO calculation. Below we show the  $Q^2 - x_{Bj}$  surface for one of those values of  $p_m$  located near the minimum observed in the measured  $A_{LT'}(p_m)$ . The full set of plots can be seen at <https://facultystaff.richmond.edu/~ggilfoyl/research/wvoCalcs1.pdf>.

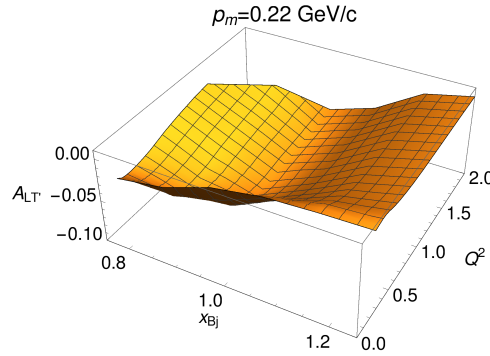


Figure 4: Surface plot of  $Q^2 - x_{Bj}$  from the WVO calculation for  $A_{LT'}(p_m = 0.22 \text{ GeV}/c, Q^2, x_{Bj})$ .

10. We now take the WVO, calculated  $Q^2 - x_{Bj}$  surface at a particular value of  $p_m$  (*i.e.*  $A_{LT'}^{WVO}(p_m, Q^2, x_{Bj})$ ) and multiply it by the probability density  $P(Q^2, x_{Bj})$  taken from our data (see the right-hand panels in Figs 2-3). The results of these calculations for the two torus polarities are shown in Fig 5 for  $p_m = 0.22 \text{ GeV}/c$  which is near the minimum in the measured  $A_{LT'}$  (same value of  $p_m$  used for Fig 4). The figure shows the normal torus polarity in the left-hand panel and the reversed polarity in the right-hand panel.

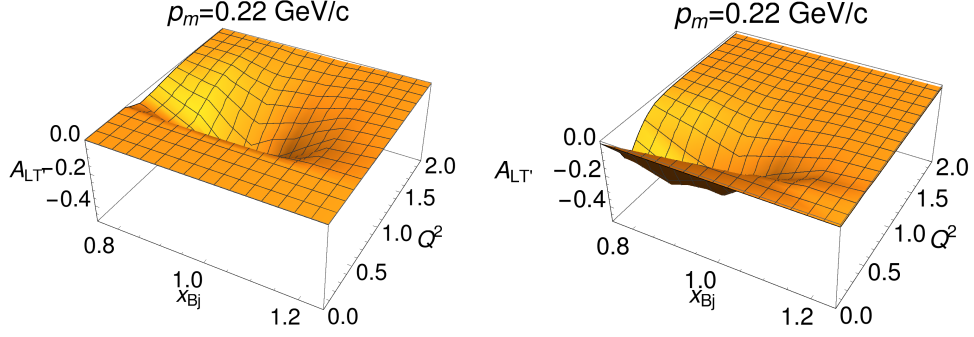


Figure 5: WVO calculation weighted by the data, *i.e.* the surface plots represent the argument of the integral in Equation 3  $A_{LT'}^{WVO}(p_m = 0.22 \text{ GeV}/c, Q^2, x_{Bj}) \times P(Q^2, x_{Bj})$  for normal torus polarity (left-hand panel) and reversed torus polarity (right-hand panel).

11. The surfaces in Fig 5 are then integrated over  $Q^2$  and  $x_{Bj}$  to get the final, theoretical value of  $A_{LT'}^{WVO}(p_m = 0.22 \text{ GeV}/c)$  for each torus polarity setting. See Eq. 3. There are sets of plots like these for each value of  $p_m$  that can be seen by seen at the following sites <https://facultystaff.richmond.edu/~ggilfoyl/research/wvoCalcsWeighted2.6n.pdf> for the normal torus polarity calculation and for the reversed torus polarity calculation at <https://facultystaff.richmond.edu/~ggilfoyl/research/wvoCalcsWeighted2.6r.pdf>.
12. The final version of the WVO  $A_{LT'}$  calculation is compared with our previous method below in Fig 6. For each torus polarity, the new  $A_{LT'}^{WVO}$  in red is close to the previous

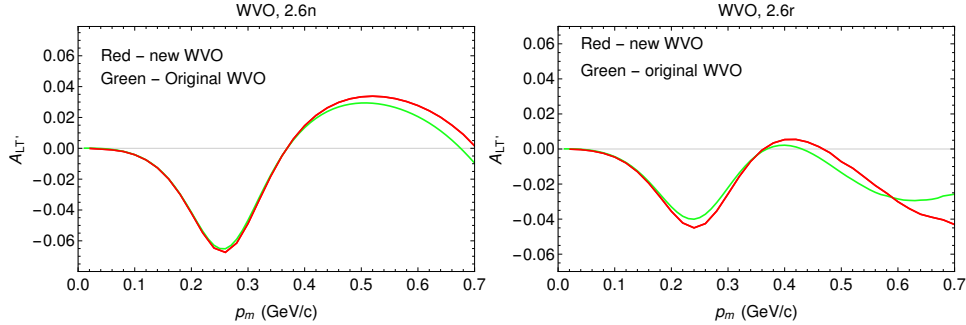


Figure 6: Comparison of theory curve weighted by two different methods for 2.6n and 2.6r.

one in green. For the reversed torus polarity the curves start to diverge at large  $p_m$ , but this is where the uncertainties on the measured  $A_{LT'}$  are large. It is, perhaps not a huge surprise the curves in Fig 6 are similar. The original distributions in  $Q^2$  and  $x_{Bj}$  for quasielastic kinematics were not very broad so the averaging procedure we used before was dominated by a few of the WVO curves near the peak of those distributions.